

Ultrafast terahertz response of multilayer graphene in the nonperturbative regime

P. Bowlan, E. Martinez-Moreno, K. Reimann, T. Elsaesser, and M. Woerner
Max-Born-Institut für Nichtlineare Optik und Kurzzeitspektroskopie, 12489 Berlin, Germany
 (Received 18 June 2013; published 27 January 2014)

The nonlinear dynamics of electrons in multilayer epitaxial graphene is investigated by time-resolved terahertz (THz) spectroscopy in a regime where the interaction of electrons with the external field dominates over scattering processes. The predominantly coherent electron response to the THz field involves both intra- and interband currents, leading to coherently driven interband transitions of carriers and to the generation of higher harmonics of the THz carrier frequency. The overall behavior of the graphene layers is always absorptive, even after generation of an initial electron-hole distribution by femtosecond midinfrared excitation. The results are in agreement with theoretical calculations of the nonperturbative THz response.

DOI: [10.1103/PhysRevB.89.041408](https://doi.org/10.1103/PhysRevB.89.041408)

PACS number(s): 72.80.Vp, 72.20.Ht, 73.22.Pr, 78.47.J–

Graphene, a layer of carbon atoms in a hexagonal arrangement, has a peculiar band structure, which results in novel transport properties such as electron velocities independent of carrier energy [1]. Linear transport properties and nonequilibrium carrier dynamics have been studied extensively, the latter mainly by ultrafast nonlinear optical methods [2–9]. In contrast, high-field transport in which the coupling of electrons to the applied electric field represents the strongest interaction, has been explored to a much lesser extent. In k space, the relevant electrons for transport are those close to the K and K' (Dirac) points, where the band gap disappears.

Figure 1 shows graphene's band structure close to the K and K' points as a function of the x component of the carrier wave vector \vec{k} . According to the acceleration theorem $d\vec{k}/dt = -e\vec{E}(t)/\hbar$, the electric field $E(t)$ of a THz pulse polarized in the x direction moves an electron back and forth along k_x on a trajectory $k_x(t) = eA_x(t)/\hbar$ determined by the vector potential $A_x(t)$ (e is the elementary charge). For high-field transport the amplitude of this motion is large compared to the initial $|k_x - K_x|$. k_y remains constant during this motion and, thus, the valence and conduction bands along $k_x - K_x$ show a hyperbolic k dependence. For an electron with an initial \vec{k} with $|k_y - K_y| \gg \omega_{\text{THz}}/2v_F$, the intraband motion dominates the response to the applied THz field. In contrast, electrons residing initially at k vectors with $|k_y - K_y| \ll \omega_{\text{THz}}/2v_F$ perform predominantly combined inter- and intraband trajectories [Fig. 1(b)].

The conelike band structure (Fig. 1) results in a constant optical interband absorption of $\pi\alpha = 0.023$ per layer (α is the fine structure constant) over a large frequency range [6,10,11]. This corresponds to an interband momentum matrix element p independent of transition energy $\hbar\omega$ [12], while the interband dipole matrix element $d = -iep/(m\omega)$ [13] is proportional to the inverse of the transition frequency (m is the electron mass). At a frequency of 2 THz, the interband transition dipole has a very high value of $d = e \times 80$ nm. The interband Rabi frequency $\Omega = d \times E/\hbar$ is equal to the THz carrier frequency for a THz electric-field amplitude of $E = 1$ kV/cm. Therefore, the light-matter interaction in graphene is nonperturbative with even moderately strong THz pulses [14–17], while at optical frequencies graphene behaves similar to other materials [18].

For a finite density of conduction band electrons and valence band holes, both intra- and interband currents can contribute to transport. In contrast to this picture, most

experiments, in particular in the THz range, have been interpreted only in terms of Drude-like intraband currents [5–8,10,11,19–25]. Here, we study the interplay of intra- and interband high-field transport in a multilayer graphene sample. We drive the electrons with strong THz fields, so that the light-matter interaction is nonperturbative and the coupling of electrons to the external driving field is much stronger than other scattering processes. We demonstrate predominantly coherent transport with both intra- and interband components. The highly nonlinear electron response results in the generation of higher harmonics of the THz carrier frequency and coherently driven interband transitions of carriers.

In the experiments, we study an epitaxial 45-layer graphene sample grown by C-face epitaxy on 4H-SiC (from Graphene Works). This sample shows negligible electronic coupling between the layers [26,27] and, thus, behaves essentially as 45 adjacent single layers. The layer stack has a total thickness of 13.2 nm, much smaller than the THz wavelength, so that all layers experience the same applied electric field.

Two-dimensional (2D) THz spectroscopy with two phase-locked THz pulses [28–30] or a midinfrared (MIR) pump-THz-probe scheme are applied in the time-resolved experiments. The THz pulses with a spectrum extending from 1 to 3 THz and MIR pulses at 14.5 THz (photon energy 60 meV) were derived from the output of an amplified Ti:sapphire laser system by difference frequency generation in GaSe [31]. They are detected in amplitude and phase by electro-optic sampling [32–34] in ZnTe [data in Figs. 2(f), 3, and 4] or—with a larger detection bandwidth—in GaP [data in Figs. 2(a)–2(e)]. The maximum electric-field amplitude of the THz pulses was between 0.2 and 50 kV/cm in the different measurements.

The THz transmission of the graphene stack, which is given by $\int E_{SG}(t)^2 dt / \int E_S(t)^2 dt$, was measured at sample temperatures of $T = 50$ and 300 K in a single-beam experiment using pulses with amplitudes between 0.2 and 30 kV/cm [$E_S(t)$ is the THz transient through the substrate alone, and $E_{SG}(t)$ the transient through both the substrate and the graphene; see Fig. 2(a)]. In the linear regime, the transmitted intensity at $T = 50$ K is 56% [Fig. 2(f)]. This value is below the transmission from quantum absorption (for our sample, 65%). The linear transmission decreases with temperature, and at $T = 300$ K it is 36%. The values given here are averaged over the incident THz spectrum between 1

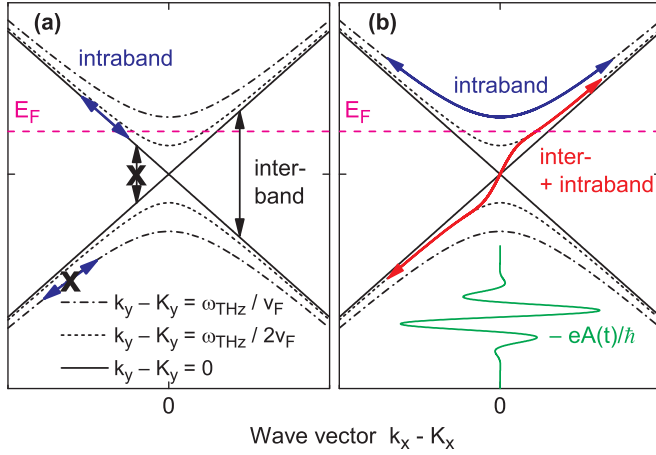


FIG. 1. (Color online) (a) Schematic band structure of graphene close to the K point where the band gap disappears. For a finite Fermi energy E_F , interband transitions with transition frequencies $\hbar\omega < 2E_F$ are forbidden, but intraband transitions and currents of electrons and holes occur. (b) For strong driving fields, there are combined inter- and intraband currents. The region of k space covered by carrier motions is determined by the vector potential $A(t)$.

and 3 THz. A more detailed analysis of the linear spectra to be presented elsewhere shows that the experimental spectra are well reproduced by the Drude transmission [6,7,10,11,19–21] with an average Fermi energy $\bar{E}_F = 24$ meV and a scattering time $T_s = 40$ fs, both being temperature independent [35]. The transmission of the graphene sample decreases with increasing incident THz field strength [Fig. 2(f)]. This behavior agrees very well with the theoretical results (solid line) [36].

The THz transients $E_{SG}(t)$ and $E_S(t)$ in Fig. 2(a) are in the strongly nonperturbative regime. In Fig. 2(b) we show the graphene response, i.e., the difference $E_{em}(t) = E_{SG}(t) - E_S(t)$, after high-pass filtering. This transient exhibits oscillations at frequencies higher than the fundamental THz carrier frequency. Such components are clearly beyond the noise level, which is evident from the data before the pulse, e.g., at 0.6 ps. To demonstrate that these high-frequency oscillations are not an artifact from the high-pass filtering, we also show the difference assuming Drude transmission using the same filtering (dashed line). The power spectrum $|E_{em}(\omega)|^2$ [Fig. 2(c)] clearly shows the first, third, and fifth harmonics with a ratio of $1 : 3 \times 10^{-3} : 5 \times 10^{-4}$. The strength of the higher harmonics is well below the dynamic range of the experiments of Ref. [37] and substantially smaller than the ratio of $1 : 1/9 : 1/25$ theoretically predicted in Ref. [14]. In Fig. 2(d) the spectral amplitudes $|E_{em}(\omega)|$ are shown for three different experimental conditions. Both decreasing the incident field amplitude and increasing the temperature leads to a decrease of the third and fifth harmonics of the THz fundamental. In Fig. 2(e) we show the dependence of the fundamental and the third and fifth harmonics of the graphene response on the incident field amplitude. The values are obtained from the experimental spectra by Gaussian fits with both the center frequencies and the widths fixed [the center frequency of the third (fifth) harmonic is three (five) times the center frequency of the fundamental and has $\sqrt{3}$ ($\sqrt{5}$) times the fundamental width].

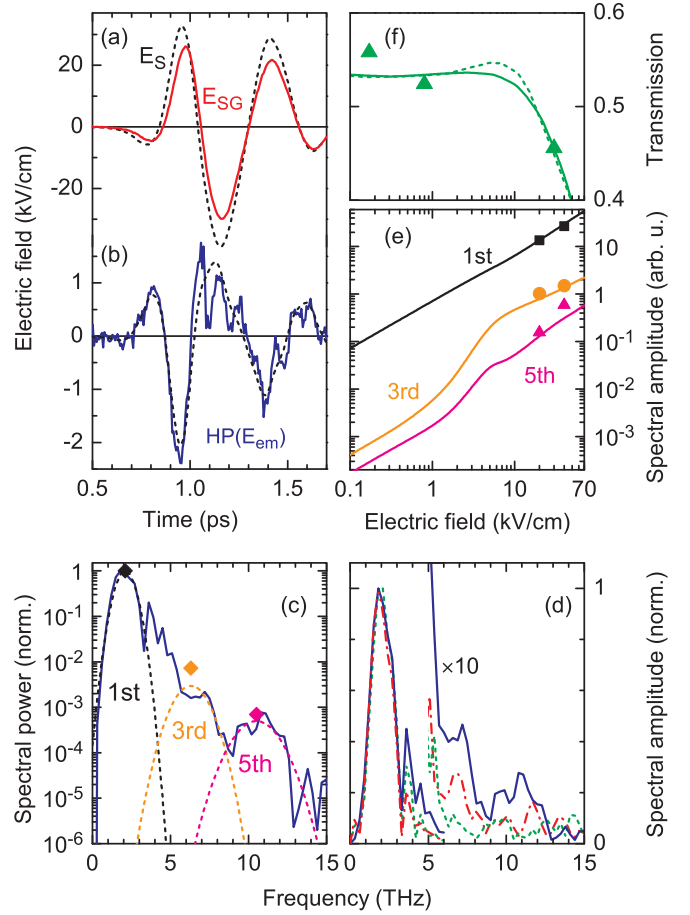


FIG. 2. (Color online) (a) Electric-field transients through the substrate (E_S , dashed line) and through the substrate and the graphene (E_{SG} , solid line) at $T = 50$ K. (b) Graphene response: The difference $E_{em} = E_{SG} - E_S$, after high-pass filtering (HP) (solid line). The dashed line shows the result from a Drude transmission with the same filtering. (c) Solid line: Spectral power $|E_{em}(\omega)|^2$ from the data in (a) and (b). The dashed lines show Gaussian fits of the fundamental, the third, and the fifth harmonic. The symbols give the theoretical values taken from Fig. 6 of Ref. [16]. (d) Spectral amplitudes $|E_{em}(\omega)|$ of the graphene response for the data in (a) and (b) (solid line), for a measurement with half the incident field amplitude (dashed line), and for a measurement at $T = 300$ K (dashed-dotted line). (e) Spectral amplitudes of the graphene response at the fundamental, the third, and the fifth harmonics as a function of the incident field amplitude. The symbols are experimental results, and the solid lines are calculations. (f) Transmission as a function of the incident field amplitude at $T = 50$ K (triangles, experimental results; dashed line, theory using plane waves; solid line, theory including the electric-field variation across the THz beam).

In the 2D experiments, two phase-locked pulses A and B interact with the graphene sample in a collinear geometry. Their electric fields transmitted through the sample are measured as a function of the real time t and of the delay τ between pulses A and B. The nonlinear signal is the difference between the electric field when both pulses are present minus the electric fields of the two pulses alone: $E_{NL}(t, \tau) = E_{AB}(t, \tau) - E_A(t, \tau) - E_B(t)$. After a 2D Fourier transform of $E_{NL}(t, \tau)$, different contributions to the nonlinear

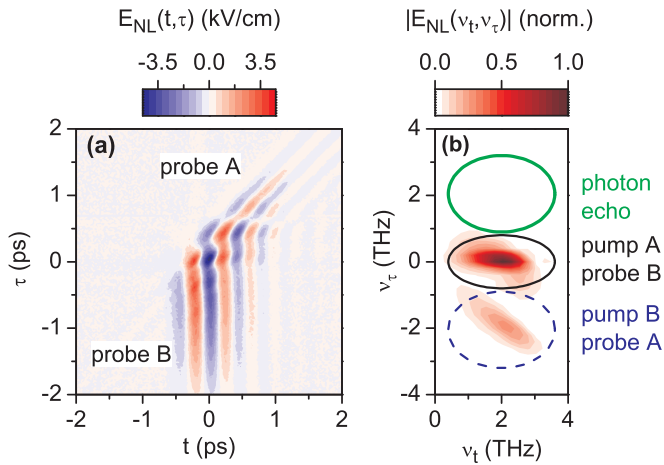


FIG. 3. (Color online) Nonlinear signal from graphene at room temperature from the 2D THz measurements. (a) shows the signal in the time domain as a function of real time t and delay τ , and (b) in the frequency domain after a 2D Fourier transform. The nonlinear signal shows only pump-probe signals; photon-echo signals are absent.

signal, such as pump-probe and photon-echo components, can be separated in 2D frequency space. For further details, see Refs. [28–30]. In the MIR-THz pump-probe experiments, the MIR pump pulse generates electron-hole pairs, which contribute to charge transport driven by the THz probe pulse.

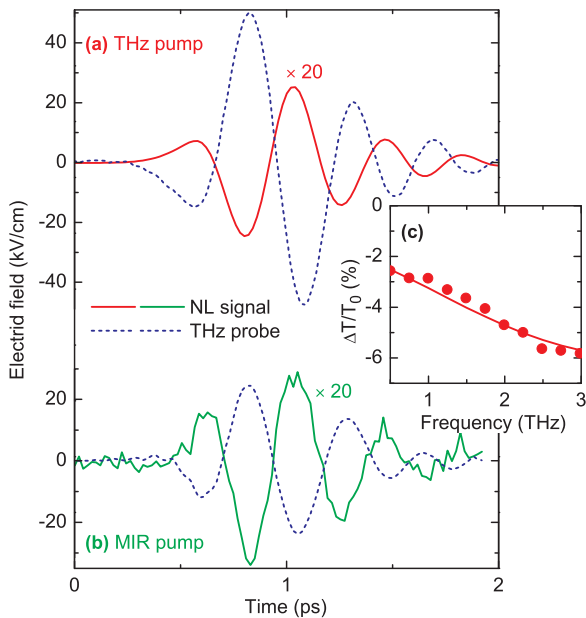


FIG. 4. (Color online) Nonlinear THz response of graphene at room temperature after excitation with (a) 2 THz (8 meV) and (b) midinfrared (60 meV) pump pulses. The dashed lines are the electric-field transients of the transmitted THz probe pulse, and the solid lines are the transients of the nonlinear signal. (c) Symbols: Spectrally resolved change in transmission after THz excitation divided by the transmission without excitation. The solid line shows the calculated spectrum for a 9% increase of the number of carriers and a decrease of T_s from 40 to 37 fs.

Again, the transmitted THz field is measured in amplitude and phase to map the nonlinear response of the graphene sample.

Results of the 2D experiment with the graphene sample at $T = 300$ K are summarized in Fig. 3. Figure 3(a) shows the nonlinear signal in the time domain as a function of the real time t and the delay τ between the THz pulses A and B, while the 2D frequency domain spectrum derived by a 2D Fourier transform is plotted in Fig. 3(b). The 2D spectrum displays two pump-probe signals, in which either pulse A or B serves as the pump pulse. It is important to note that a photon-echo signal is completely absent, although the data of Fig. 2 clearly point to the coherent character of the graphene response.

In Fig. 4, we present the phase-resolved pump-probe response measured under different experimental conditions. Transients observed in a 2D THz experiment at $T = 300$ K are shown in Fig. 4(a), whereas the data in Fig. 4(b) were measured with MIR excitation at 14.5 THz (MIR electric-field amplitude 40 kV/cm, pulse length 0.3 ps) and THz probe pulses. In both cases, the incident THz probe field (dashed line) and the nonlinear THz field E_{NL} are shifted in phase by π , indicating induced absorption. Figure 4(c) shows a differential transmission spectrum after THz excitation (symbols) and the calculated response (solid line).

Our results demonstrate the coherent nature of the nonlinear response, which is most clearly manifested in the generation of higher harmonics of the THz carrier frequency. This behavior originates from the strong nonperturbative interaction between the THz driving field and the electrons, which dominates over electron-electron and electron-lattice interactions that underlie incoherent scattering processes. Under the present conditions, carrier transport is in the quantum-kinetic regime. Two other striking features of the nonlinear response are (i) the observation of an overall absorptive response of the graphene sample in a very wide range of electric-field strengths from 0.2 up to 50 kV/cm, and (ii) the absence of photon-echo signals in the 2D spectra.

In our graphene sample, the nonzero density of electrons in the conduction band and holes in the valence band allows for inducing both intra- and interband currents with the strong external THz field. Intraband currents are connected with motions of conduction band electrons and valence band holes over a wide range in k space. Due to graphene's band structure, the effective electron mass increases at large k values, and, thus, the real part of the conductivity decreases. Concomitantly, the intraband THz absorption decreases, a behavior in contrast to the experimentally observed absorption increase. The latter points to a significant contribution of interband currents (cf. Fig. 1), by which electrons move coherently between valence and conduction bands. This mechanism enhances the concentration of free carriers and, thus, both the conductivity and the THz absorption. In the interplay of intra- and interband transport, a particular electron contributes to both currents, depending on the region in k space its motion covers momentarily. It is important to note that the overall absorptive THz response is independent of the particular excitation process by which the initial carrier populations in the conduction and valence bands are generated. Femtosecond interband excitation by midinfrared pulses [cf. Fig. 4(b)] increases the carrier density contributing to the overall current and, thus, results in enhanced absorption.

Also the absence of a photon-echo signal is due to the nonperturbative character of the nonlinear interaction, for which the interband Rabi frequency is significantly larger than the THz carrier frequency. The interband Rabi frequency is different at each point in k space, due to both the k -dependent interband dipole moment and to the different electric-field amplitudes at different interband transition frequencies. Thus, a coherent rephasing of the different components of the interband polarization by interactions with the THz driving field is impossible and the total photon-echo signal is negligible.

Both intra- and interband transitions are important for the generation of higher harmonics. Due to graphene's band structure, the oscillating intraband polarization generated by an essentially sinusoidal driving field contains a wide frequency spectrum including higher harmonics. While the direct contribution of the interband current to the generation of higher harmonics is weak, interband transitions are nevertheless important since they determine the density of electrons and holes available for intraband transitions. The exact shape of the carrier distribution, a topic of many ultrafast optical studies of graphene [2–9], plays a minor role as the width of the distribution is small compared to the energy range covered by its trajectory.

To account for the experimental results, we performed model calculations based on the theory developed by Ishikawa [16,17]. The theory contains graphene's electronic band structure and the interaction with the external THz field. Scattering processes such as electron-phonon, electron-impurity, and electron-electron scattering are neglected. Considering the fact that these scattering processes are responsible, e.g., for the Drude width in linear absorption [5–8,10,11,19–25], for ultrafast thermalization [9] and cooling [38], this approach needs to be justified. Under our experimental conditions, the optical inter- and intraband transition rates induced by coupling to the strong THz driving field (amplitude 20–30 kV/cm) are of the order of several 10^{14} s $^{-1}$, much higher than the electron scattering rates due to the interactions mentioned [39]. As a measure for the latter, we consider the Drude scattering rate $1/T_s$, encompassing all relevant scattering processes of electrons. An analysis of our data gives a value of $1/T_s \simeq 2.5 \times 10^{13}$ s $^{-1}$, which is an order of magnitude smaller than the optical transition rates and remains essentially unchanged in the presence of the strong THz field [see the solid line in Fig. 4(c)], in agreement with Ref. [40].

The equations of Ishikawa's theory [16,17] describe the response of a single graphene layer (i.e., intraband plus interband current) to a given THz driving field. However,

in Refs. [16,17] the energy transfer from the sample to the electromagnetic field is neglected. To include this energy transfer and to account correctly for energy conservation requires the introduction of the radiation reaction field [41,42]. For the THz response of a multilayer graphene sample this is particularly simple, since the thickness of the entire stack $d \approx 10$ nm is orders of magnitude smaller than the involved wavelengths. As a result, each graphene layer experiences the same driving field, which is the transmitted field through the sample $E_{tr} = E_{in} + E_{em}$ (without the radiation reaction field the driving field is equal to the incident field). E_{tr} consists of both the incident field E_{in} and the field E_{em} emitted by the stack of graphene layers, which is determined by the sum of intra- and interband currents in all layers. For graphene on a substrate one has to introduce an additional field $E_{sub}(t) = E_{tr}(t)(1 - n_{sub})/2$ emitted due to the refractive index jump at the interface [27].

Using Ishikawa's theory [16,17] with the modification described above, we calculated transients for multilayer epitaxial graphene (Figs. 2–4). The theory fully confirms the physical picture of electron-hole generation via interband trajectories as the main mechanism for the observed induced absorption. Without the interband polarization, the nonlinear induced absorption vanishes. In contrast to Ref. [14], this treatment predicts a ratio of harmonic powers in agreement with experiment [Fig. 2(e)]. Furthermore, the theory accounts for the quantum absorption in the linear regime and for the generation of higher harmonics [16,17]. The absence of the photon echo is also predicted by the theory.

In conclusion, we studied the nonlinear dynamics of electrons in multilayer epitaxial graphene by time-resolved THz spectroscopy in a regime where the interaction of electrons with the external field dominates over scattering processes. A physical picture solely based on graphene's band structure and light-matter interaction including the radiation reaction field fully explains the predominantly coherent electron response to the THz field. Even at low frequencies, both intra- and interband currents are involved to allow for coherently driven interband trajectories of carriers and for generating higher harmonics of the THz carrier frequency. The interband transitions explain the overall absorptive behavior of the graphene layers, even after generation of an initial electron-hole distribution by femtosecond optical excitation. The results are in agreement with theoretical calculations of the nonperturbative THz response including the radiation reaction field.

We acknowledge financial support by the Deutsche Forschungsgemeinschaft (RE 806/9-1).

-
- [1] A. H. Castro Neto, F. Guinea, N. M. R. Peres, K. S. Novoselov, and A. K. Geim, *Rev. Mod. Phys.* **81**, 109 (2009).
- [2] J. M. Dawlaty, S. Shivaraman, M. V. S. Chandrashekar, F. Rana, and M. G. Spencer, *Appl. Phys. Lett.* **92**, 042116 (2008).
- [3] D. Sun, C. Divin, C. Berger, W. A. de Heer, P. N. First, and T. B. Norris, *Phys. Rev. Lett.* **104**, 136802 (2010).
- [4] D. Sun, Z.-K. Wu, C. Divin, X. Li, C. Berger, W. A. de Heer, P. N. First, and T. B. Norris, *Phys. Rev. Lett.* **101**, 157402 (2008).
- [5] P. A. George, J. Strait, J. Dawlaty, S. Shivaraman, M. Chandrashekar, F. Rana, and M. G. Spencer, *Nano Lett.* **8**, 4248 (2008).
- [6] H. Choi, F. Borondics, D. A. Siegel, S. Y. Zhou, M. C. Martin, A. Lanzara, and R. A. Kaindl, *Appl. Phys. Lett.* **94**, 172102 (2009).

- [7] J. H. Strait, H. Wang, S. Shivaraman, V. Shields, M. Spencer, and F. Rana, *Nano Lett.* **11**, 4902 (2011).
- [8] S. Winnerl, M. Orlita, P. Plochocka, P. Kossacki, M. Potemski, T. Winzer, E. Malic, A. Knorr, M. Sprinkle, C. Berger, W. A. de Heer, H. Schneider, and M. Helm, *Phys. Rev. Lett.* **107**, 237401 (2011).
- [9] M. Breusing, S. Kuehn, T. Winzer, E. Malić, F. Milde, N. Severin, J. P. Rabe, C. Ropers, A. Knorr, and T. Elsaesser, *Phys. Rev. B* **83**, 153410 (2011).
- [10] R. R. Nair, P. Blake, A. N. Grigorenko, K. S. Novoselov, T. J. Booth, T. Stauber, N. M. R. Peres, and A. K. Geim, *Science* **320**, 1308 (2008).
- [11] J. M. Dawlaty, S. Shivaraman, J. Strait, P. George, M. Chandrashekar, F. Rana, M. G. Spencer, D. Veksler, and Y. Chen, *Appl. Phys. Lett.* **93**, 131905 (2008).
- [12] A. Grüneis, R. Saito, G. G. Samsonidze, T. Kimura, M. A. Pimenta, A. Jorio, A. G. Souza Filho, G. Dresselhaus, and M. S. Dresselhaus, *Phys. Rev. B* **67**, 165402 (2003).
- [13] M. Schubert and G. Weber, *Quantentheorie* (Spektrum, Heidelberg, 1993).
- [14] S. A. Mikhailov, *Europhys. Lett.* **79**, 27002 (2007).
- [15] A. R. Wright, X. G. Xu, J. C. Cao, and C. Zhang, *Appl. Phys. Lett.* **95**, 072101 (2009).
- [16] K. L. Ishikawa, *Phys. Rev. B* **82**, 201402(R) (2010). Figure 6 in this reference shows $|\omega J(\omega)|^2$, whereas our Fig. 2(c) shows $|E_{em}(\omega)|^2$, which in our geometry is proportional to $|J(\omega)|^2$, i.e., the two figures differ by ω^2 .
- [17] K. L. Ishikawa, *New J. Phys.* **15**, 055021 (2013).
- [18] N. Kumar, J. Kumar, C. Gerstenkorn, R. Wang, H.-Y. Chiu, A. L. Smirl, and H. Zhao, *Phys. Rev. B* **87**, 121406 (2013).
- [19] T. Stauber, N. M. R. Peres, and A. K. Geim, *Phys. Rev. B* **78**, 085432 (2008).
- [20] H. Yan, F. Xia, W. Zhu, M. Freitag, C. Dimitrakopoulos, A. A. Bol, G. Tulevski, and P. Avouris, *ACS Nano* **5**, 9854 (2011).
- [21] J. Horng, C.-F. Chen, B. Geng, C. Girit, Y. Zhang, Z. Hao, H. A. Bechtel, M. Martin, A. Zettl, M. F. Crommie, Y. R. Shen, and F. Wang, *Phys. Rev. B* **83**, 165113 (2011).
- [22] M. Orlita, C. Faugeras, P. Plochocka, P. Neugebauer, G. Martinez, D. K. Maude, A.-L. Barra, M. Sprinkle, C. Berger, W. A. de Heer, and M. Potemski, *Phys. Rev. Lett.* **101**, 267601 (2008).
- [23] P. Neugebauer, M. Orlita, C. Faugeras, A.-L. Barra, and M. Potemski, *Phys. Rev. Lett.* **103**, 136403 (2009).
- [24] J. Karch, C. Drexler, P. Olbrich, M. Fehrenbacher, M. Hirmer, M. M. Glazov, S. A. Tarasenko, E. L. Ivchenko, B. Birkner, J. Eroms, D. Weiss, R. Yakimova, S. Lara-Avila, S. Kubatkin, M. Ostler, T. Seyller, and S. D. Ganichev, *Phys. Rev. Lett.* **107**, 276601 (2011).
- [25] Y.-F. Lao, A. G. U. Perera, K. Shepperd, F. Wang, E. H. Conrad, and M. D. Williams, *Appl. Phys. Lett.* **102**, 231906 (2013).
- [26] J. Hass, F. Varchon, J. E. Millán-Otoya, M. Sprinkle, N. Sharma, W. A. de Heer, C. Berger, P. N. First, L. Magaud, and E. H. Conrad, *Phys. Rev. Lett.* **100**, 125504 (2008).
- [27] M. Sprinkle, D. Siegel, Y. Hu, J. Hicks, A. Tejada, A. Taleb-Ibrahimi, P. Le Fèvre, F. Bertran, S. Vizzini, H. Enriquez, S. Chiang, P. Soukiassian, C. Berger, W. A. de Heer, A. Lanzara, and E. H. Conrad, *Phys. Rev. Lett.* **103**, 226803 (2009).
- [28] W. Kuehn, K. Reimann, M. Woerner, and T. Elsaesser, *J. Chem. Phys.* **130**, 164503 (2009).
- [29] W. Kuehn, K. Reimann, M. Woerner, T. Elsaesser, and R. Hey, *J. Phys. Chem. B* **115**, 5448 (2011).
- [30] M. Woerner, W. Kuehn, P. Bowlan, K. Reimann, and T. Elsaesser, *New J. Phys.* **15**, 025039 (2013).
- [31] K. Reimann, *Rep. Prog. Phys.* **70**, 1597 (2007).
- [32] Q. Wu and X.-C. Zhang, *Appl. Phys. Lett.* **67**, 3523 (1995).
- [33] A. Leitenstorfer, S. Hunsche, J. Shah, M. C. Nuss, and W. H. Knox, *Appl. Phys. Lett.* **74**, 1516 (1999).
- [34] T. Bartel, P. Gaal, K. Reimann, M. Woerner, and T. Elsaesser, *Opt. Lett.* **30**, 2805 (2005).
- [35] Because of the symmetry of the graphene band structure near the K point we can determine the magnitude, but not the sign, of E_F . According to Refs. [3,4,43] we take $E_F \geq 0$.
- [36] The slight transmission increase (dashed line) around 5 kV/cm is caused by a reflectivity decrease, while the absorption increases monotonically. Integrating over the different field amplitudes present in the waist of the THz beam smears out the transmission maximum (solid line).
- [37] M. J. Paul, Y. C. Chang, Z. J. Thompson, A. Stickel, J. Wardini, H. Choi, E. D. Minot, T. B. Norris, and Y.-S. Lee, *New J. Phys.* **15**, 085019 (2013).
- [38] M. W. Graham, S.-F. Shi, D. C. Ralph, J. Park, and P. L. McEuen, *Nat. Phys.* **9**, 103 (2013).
- [39] To compare light-matter interaction rates with scattering processes, see Eq. (6.3.5) of T. Kuhn, in *Theory of Transport Properties of Semiconductor Nanostructures*, edited by E. Schöll (Chapman & Hall, London, 1998), pp. 173–214.
- [40] L. M. Malard, K. F. Mak, A. H. C. Neto, N. M. R. Peres, and T. F. Heinz, *New J. Phys.* **15**, 015009 (2013).
- [41] T. Stroucken, A. Knorr, P. Thomas, and S. W. Koch, *Phys. Rev. B* **53**, 2026 (1996).
- [42] T. Shih, K. Reimann, M. Woerner, T. Elsaesser, I. Waldmüller, A. Knorr, R. Hey, and K. H. Ploog, *Phys. Rev. B* **72**, 195338 (2005).
- [43] F. Varchon, R. Feng, J. Hass, X. Li, B. N. Nguyen, C. Naud, P. Mallet, J.-Y. Veuillen, C. Berger, E. H. Conrad, and L. Magaud, *Phys. Rev. Lett.* **99**, 126805 (2007).